



Thermodynamically stable ionic liquid microemulsions pioneer pathways for topical delivery and peptide application

Tianqi Liu^{a,b,1}, Ying Liu^{f,1}, Xiaoyu Zhao^{e,1}, Liguo Zhang^d, Wei Wang^d, De Bai^{a,b}, Ya Liao^c, Zhenyuan Wang^c, Mi Wang^{a,b,**}, Jiaheng Zhang^{a,b,c,*}

^a State Key Laboratory of Advanced Welding and Joining, School of Materials Science and Engineering, Harbin Institute of Technology (Shenzhen), Shenzhen, 518055, China

^b Research Center of Printed Flexible Electronics, School of Materials Science and Engineering, Harbin Institute of Technology, Shenzhen, 518055, China

^c Shenzhen Shinehigh Innovation Technology Co., Ltd., Shenzhen, 518055, China

^d Harbin Voolga Technology Co., Ltd., Harbin, 150070, China

^e CAS Key Laboratory of Quantitative Engineering Biology, Shenzhen Institute of Synthetic Biology, Shenzhen Institutes of Advanced Technology, Chinese Academy of Sciences, Shenzhen, 518055, China

^f Department of Chemistry, College of Sciences, Northeastern University, Shenyang, 110819, China

ARTICLE INFO

Keywords:

Bio-based ionic liquids

Copper peptides

Microemulsion

Hair regeneration

Transdermal delivery

ABSTRACT

Copper peptides (GHK-Cu) are a powerful hair growth promoter with minimal side effects when compared with minoxidil and finasteride; however, challenges in delivering GHK-Cu topically limits their non-invasive applications. Using theoretical calculations and pseudo-ternary phase diagrams, we designed and constructed a thermodynamically stable ionic liquid (IL)-based microemulsion (IL-M), which integrates the high drug solubility of ILs and high skin permeability of microemulsions, thus improving the local delivery of copper peptides by approximately three-fold while retaining their biological function. Experiments in mice validated the effectiveness of our proposed IL-M system. Furthermore, the exact effects of the IL-M system on the expression of growth factors, such as vascular endothelial growth factor, were revealed, and it was found that microemulsion increased the activation of the Wnt/ β -catenin signaling pathway, which includes factors involved in hair growth regulation. Overall, the safe and non-invasive IL microemulsion system developed in this study has great potential for the clinical treatment of hair loss.

1. Introduction

Currently, the clinical treatment of hair loss primarily includes hair follicle transplantation and drug therapy [1–4]. However, hair follicle transplantation is not widely applicable owing to its high cost, invasiveness, and limited donor availability [5–7]. Therefore, medications are widely used due to their convenience and painlessness. Currently, minoxidil and finasteride are the major hair growth promoters approved by the Food and Drug Administration (FDA). Specifically, Minoxidil can prolong the anagen phase of hair follicles and promote hair growth by expanding blood vessel networks in the scalp and enhancing local blood

circulation and nutrient supply [8,9]. Finasteride is a reductase inhibitor that suppresses the activity of 5 α reductase *in vivo*, thus reducing dihydrotestosterone concentrations, attenuating hair follicle damage, and preventing hair loss [10–12].

However, currently available medications all cause significant adverse effects [9,13,14]. Specifically, minoxidil affects the cardiovascular system and tends to cause tachycardia [9], while the side effects of finasteride include gynecomastia, feminization, suppressed libido, and sperm malformation [15]. Therefore, there is a need for more efficient and safer treatment modalities. Copper peptides (GHK-Cu) are complexes composed of glycyl-L-histidyl-L-lysine tripeptides (GHK) and

Peer review under responsibility of KeAi Communications Co., Ltd.

* Corresponding author. State Key Laboratory of Advanced Welding and Joining, School of Materials Science and Engineering, Harbin Institute of Technology (Shenzhen), Shenzhen, 518055, China.

** Corresponding author. State Key Laboratory of Advanced Welding and Joining, School of Materials Science and Engineering, Harbin Institute of Technology (Shenzhen), Shenzhen, 518055, China.

E-mail addresses: wangmi@hit.edu.cn (M. Wang), zhangjiaheng@hit.edu.cn (J. Zhang).

¹ These authors contributed equally to this work.

<https://doi.org/10.1016/j.bioactmat.2023.10.002>

Received 14 June 2023; Received in revised form 9 September 2023; Accepted 1 October 2023

2452-199X/© 2023 The Authors. Publishing services by Elsevier B.V. on behalf of KeAi Communications Co. Ltd. This is an open access article under the CC BY-NC-ND license (<http://creativecommons.org/licenses/by-nc-nd/4.0/>).

divalent copper [16–18]. They can promote hair growth by (i) stimulating fibroblasts to produce vascular endothelial growth factor (VEGF) and thus promote the formation of new blood vessels around hair follicles to provide the nutrients required for growth [19–22]; (ii) inhibiting the generation of transforming growth factor beta, which prevents premature conversion of hair follicles from the anagen to the regressive phase [23–26]; and (iii) promoting the proliferation of dermal papilla cells and inhibiting their apoptosis to stimulate the growth of hair follicles and hairs [5,27,28].

However, everything has both sides, copper element exists in a metastable valence state in copper peptides, which results in high reactivity and sensitivity to pH, antioxidants, chelating agents, and other factors [29–31]. In addition, copper peptides are highly hydrophilic and are minimally absorbed by the skin when applied topically [32]. In addition, when copper peptides are injected into the dermis, approximately 95 % of the peptides are excreted by the body [33,34].

To increase the stability of copper peptides and improve their local delivery, we constructed an ionic liquid (IL) microemulsion system, which integrates the benefits of both microemulsions and ILs: (i) the microemulsion is a thermally-stable system, which increases peptide solubility and (ii) the IL enhances skin penetration and improves solubility [35]. Moreover, tartaric acid and L-carnitine were selected for the IL component because they are naturally derived and highly

biocompatible. Tartaric acid is a carboxylic acid known for its role in maintaining a weakly acidic state and suppressing microbial proliferation on the skin [36,37]. The carboxyl group in tartaric acid can be amidated with the amine group in L-carnitine to form an ester bond [38–40]. The formation of this ester bond leads to chemical bond coupling, ultimately resulting in the production of an IL, and the properties of this IL can be modulated by adjusting the ratio of tartaric acid to L-carnitine. Furthermore, previous research has shown that this combination can boost hair growth [41]. To investigate the efficacy of this strategy, we conducted a series of evaluations to investigate the optimal ratios, chemical/environmental stability, and thermal stability. A pseudo-ternary phase diagram was established to better interpret the phase stability. To further determine the biological functions of this system, multi-dimensional experimental validation was conducted using cells, *in vitro* experiments, and *in vivo* evaluations on mice. We also predicted and investigated the signal pathways underlying the efficacy of this system. Our results have potential in expanding and improving the available treatment options for hair loss.

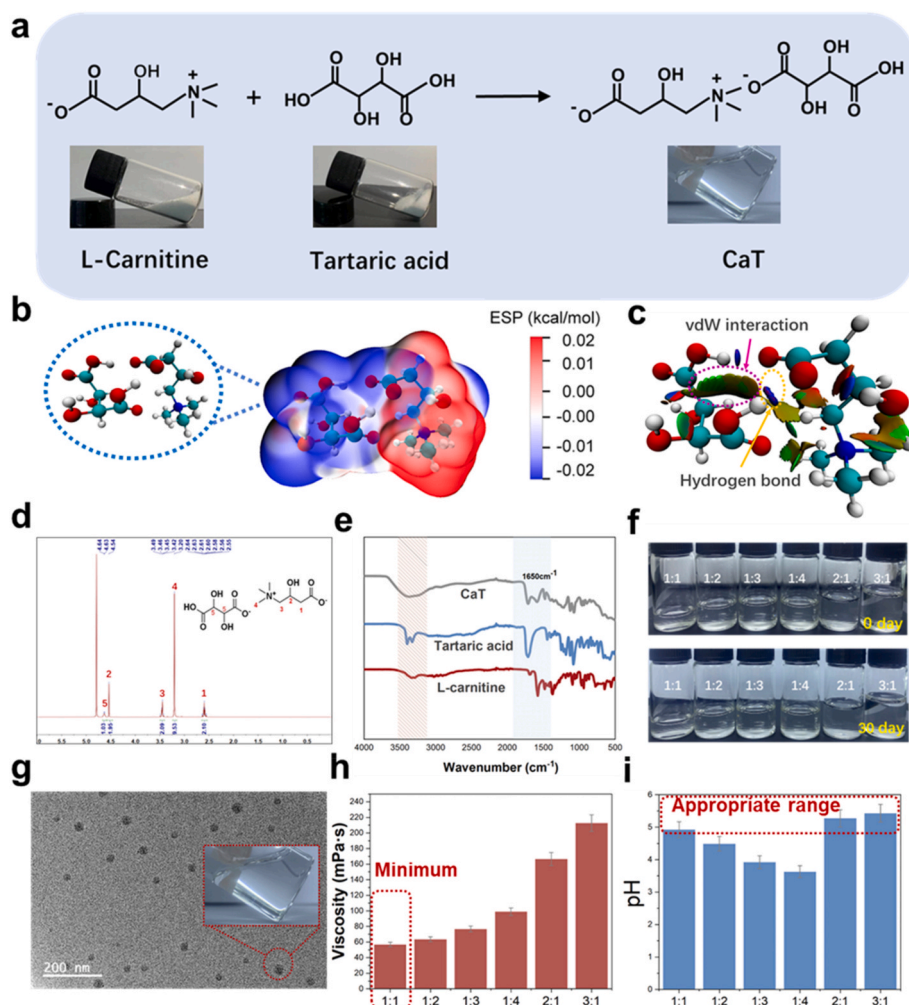


Fig. 1. Preparation, characterization, and drug-loading characteristics of bio-based ionic liquids. (a) Preparation of CaT. (b) ESP diagram of CaT (red: positively charged; blue: negatively charged). (c) RDG diagram of CaT (red: unbound overlaps; blue: strong attractive interactions; transition zone: van der Waals interactions). (d) ¹H NMR spectrum of CaT-1:1. (e) FTIR spectra of CaT-1:1, L-carnitine, and tartaric acid. (f) Photographs of CaT samples with different anion:cation molar ratios on day 0 and day 30. (g) TEM image and photograph (built-in) of CaT. Scale bar = 200 nm (h) Viscosities of CaT samples with different molar ratios of L-carnitine and tartaric acid. (i) pH values of CaT samples with different molar ratios of L-carnitine and tartaric acid.

2. Results and discussion

2.1. Preparation, characterization, and drug loading characteristics of IL

A green IL was successfully synthesized using naturally derived L-carnitine and tartaric acid (Fig. 1a). We used various ratios and found that this system possessed strong thermodynamic stability, possessed a liquid state over a wide range of ratios, and had high storage stability (Figure f).

The colors in the electrostatic potential (ESP) diagram of CaT reflect the magnitude of the surface electrostatic potential. According to modeling, during the formation of the CaT monomer, the positively charged region of L-carnitine (red) was electrostatically attracted to the negatively (blue) charged regions of tartaric acid (Fig. 1b). The reduced density gradient (RDG) diagram indicates the presence of hydrogen bonding and van der Waals interactions between L-carnitine and tartaric acid (Fig. 1c). DFT calculations indicated that CaT was stable at room temperature.

In the ^1H NMR spectrum, the area data for the methyl proton in levulinic acid (4, $-\text{CH}_3$) was used as a reference, and the ratio of its peak area to the hypomethyl group in tartaric acid (5, $\equiv\text{CH}$) was 4.5. This is consistent with the expected structure of the IL. In addition, the $\alpha\text{-H}$ of tartaric acid in CaT was located at 4.54 ppm, and the $\alpha\text{-H}$ of L-carnitine was located at 2.55–2.64 ppm; both were shifted by over 0.1 ppm compared with the $\alpha\text{-H}$ in the monomers of tartaric acid and L-carnitine, which supports that proton transfer occurred between tartaric acid and L-carnitine to form an IL (Fig. 1d). The Fourier transform infrared (FTIR) spectra of the samples contained a broad IR absorption peak at 3700–3000 cm^{-1} , corresponding to $-\text{OH}$ stretching vibrations associated with hydrogen bonding, and at 1650 cm^{-1} , corresponding to asymmetric stretching vibrations of the carboxyl (COO^-) group (Fig. 1e). These data suggest ionic interactions and the formation of hydrogen bonds between L-carnitine and tartaric acid, confirming that the IL was successfully synthesized (Fig. 1d–e, Fig. S1). The CaT samples formed using different molar ratios of the two components were clear at room temperature and exhibited some fluidity. No flocculation or precipitation occurred during 30 d of storage at room temperature, indicating that CaT had good stability (Fig. 1f).

Transmission electron microscopy (TEM) was used to investigate the microscopic morphology of CaT. The results revealed that CaT formed small spheres (Fig. 1g); this spherical nanostructure facilitates the uptake of target drug by cells and raises the drug delivery efficiency [42, 43]. Considering that the physicochemical properties of IL depend on the ratio of the two ionic components, we evaluated the physicochemical parameters of the CaT series. The viscosity of CaT with different anion:cation ratios varied from 56 to 213 mPa s, and CaT-1:1 had the lowest viscosity (56.8 mPa s) and best fluidity, indicating that the composition of IL significantly affected their viscosity (Fig. 1h). The conductivity of CaT (with changes in the anion:cation ratio) exhibited an opposite trend to that of viscosity (Figure S2). The density of CaT ranged from 1.10 to 1.25 g cm^{-3} with slight variations between samples with different anion:cation ratios, indicating that the composition of the IL only had minor effects on its density (Figure S3). Further, the pH tended to increase with increasing L-carnitine content and varied in the range of 3.6–5.5 (Fig. 1i). Thermogravimetric analysis (TGA) indicated that the decomposition temperature of CaT was between 180 and 210 $^\circ\text{C}$, and differential scanning calorimetry (DSC) revealed that the glass transition temperature (T_g) of CaT was between -12 and -25 $^\circ\text{C}$ (Figure S4 and S5). Thus, the TGA and DSC results indicated that CaT samples with anion:cation molar ratios of 1:1 and 1:2 possessed better thermal stability than the other samples. Considering the sensitivity of copper peptides to pH (4.6–7.0) and the viscosity requirement of delivery agents, we selected CaT-1:1 (anion:cation molar ratio of 1:1) for further investigations.

Copper peptides have a blue color, and the amount of copper peptides can be estimated by the hue of the system. However, when copper

peptides were mixed with CaT (solubility >130.98 g/L), their color was significantly lighter than in the aqueous solution, and the solution appeared icy-blue (Figure S6). Circular dichroism (CD) studies revealed no change in the cotton peak, suggesting that the structure of copper peptides was not affected by dissolution in CaT (Figure S7). In summary, we successfully prepared CaT and verified its feasibility as a copper peptide carrier.

2.2. Screening of IL microemulsion systems

Water-in-oil (W/O) microemulsions have been shown to be effective in topically delivering water-soluble peptides and proteins [44,45]. Given the limited local absorption of copper peptides, we prepared a CaT-based microemulsion system to enhance their stability and bioavailability. Isopropyl myristate (IPM) has been widely used in topical pharmaceutical formulations for enhancing drug solubility and biomembrane penetration [44]. Further, we used Tween 80 and Span 20 as the surfactant and co-surfactant, respectively; these are non-ionic surfactants with several hydroxyl groups and ethylene oxide linkages that can form hydrogen bonds among themselves and with ILs in mixed systems. Nonionic surfactants help overcome the incompatibility between ILs and IPM and improve the permeability of the drug formulation across tissue barriers. Therefore, we included the following components in the IL microemulsion system: CaT as the polar phase, IPM as the non-polar phase, and Tween80 and Span20 as the surfactant and co-surfactant, respectively (Fig. 2a).

We constructed pseudo-ternary phase diagrams to determine the appropriate proportions of the various components for forming a stable microemulsion. First, we set the ratios (Km, wt:wt) of Tween 80 and Span 20 (T/S) as 1:1, 1:2, 1:3, 2:1, and 2:3, and evaluated the effect of different T/S ratios on the area of the microemulsion region by constructing pseudo-ternary phase diagrams for a water/IPM system. As shown in Fig. 2b, the area of the microemulsion region was the largest when the T/S mass ratio was 1:1. Thus, the water/IPM microemulsion obtained using a 1:1 mixture (by weight) of the surfactant and cosurfactant had optimal stability, and this ratio was used for further evaluations.

Next, we prepared a series of IPM and surfactant/cosurfactant (T + S) mixtures according to the following mass ratios: 1:9, 2:8, 3:7, 4:6, 5:5, 6:4, 7:3, 8:2, and 9:1. We chose the 4:6, 7:3, and 8:2 for further experiments based on the appearance, flowability, viscosity, and stability of the microemulsions (Figure S8).

DLS studies indicated that the best emulsification effect and smallest average particle size of the dispersed phase was achieved at an IPM: T + S ratio of 8:2 (Fig. 2c). As small particle sizes of the dispersed phase facilitate local transport, we chose IPM:TS = 8:2 for subsequent evaluations. The optimal amount of CaT was determined by recording the threshold value of the system from clarification to turbidity to clarification via dropwise addition of the polar phase. Finally, stable IL microemulsions (named CaT-ME) were successfully prepared based on the aforementioned steps; the photograph of the emulsion is shown in Fig. 2d. Furthermore, the diffusion rates of a red oil-soluble dye (Sudan Red III) and blue water-soluble dye (methylene blue) were evaluated to determine the microemulsion type. A greater diffusion rate of Sudan Red III than that of methylene blue in the microemulsion was observed in the staining test, which indicated that the prepared microemulsion was of W/O type.

2.3. Performance of the IL microemulsion

TEM images of the CaT-ME showed circular, uniformly shaped particles (Fig. 3a). The zeta potentials for CaT and CaT-ME were determined to be -9.2 and -7.6 mV respectively, which suggests that the construction of the new system did not affect the potential greatly. (Fig. 3b). Furthermore, the DLS analysis revealed that the average particle size of the microemulsion was 55.21 ± 1.62 nm and that the particles were

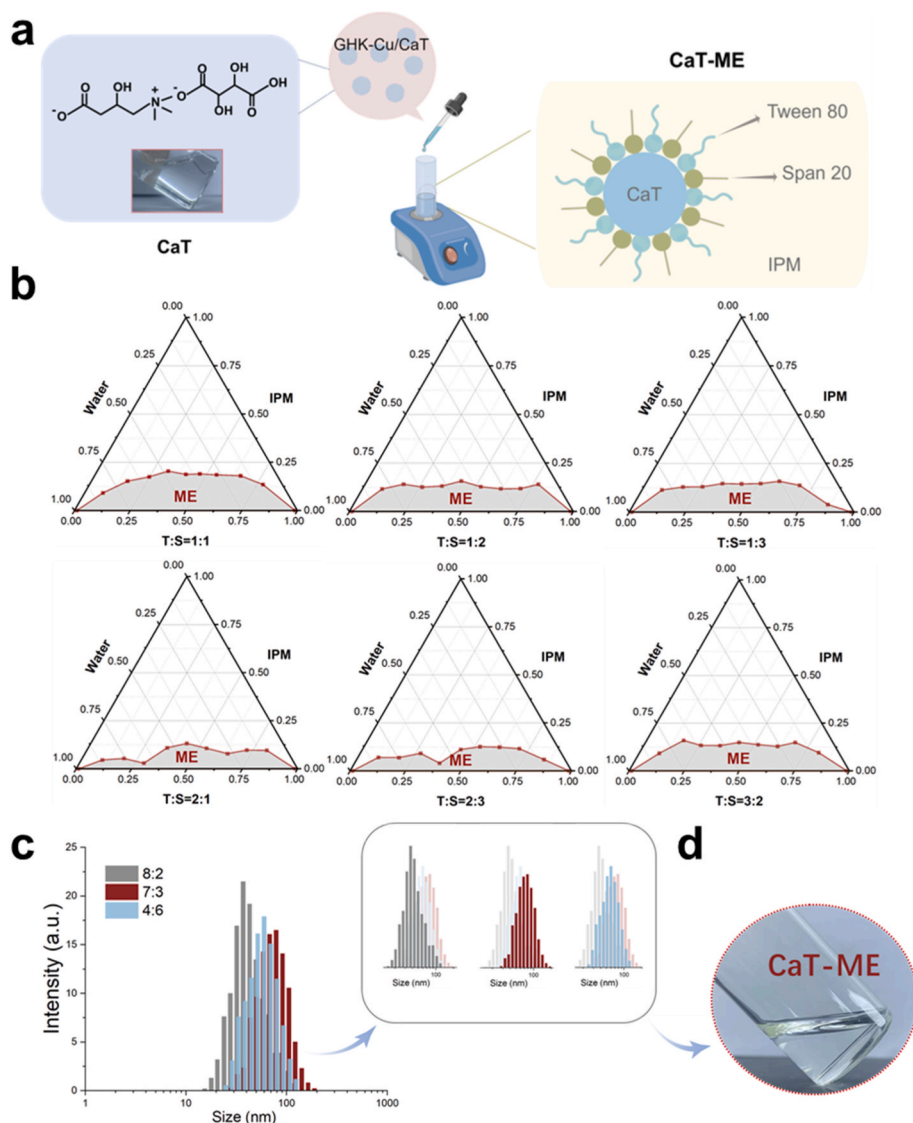


Fig. 2. Screening of ionic liquid microemulsion systems. (a) Schematic of CaT-ME preparation. (b) Pseudo-ternary phase diagram for water/isopropyl myristate (IPM) system with different surfactant (Tween 80) and co-surfactant (Span 20) ratios (gray region is the microemulsion area). (c) Particle size distribution of CaT-ME with different IPM:Tween 80+Span 20 ratios. (d) Photograph of the transparent CaT-ME.

well-dispersed, suggesting that the microemulsion were highly stable and permeable (Fig. 3c). After 50 d of storage, no emulsion breakage, flocculation, or precipitation was observed; the DLS results showed slight changes in the particle size, but robust particle dispersion, indicating the formation of a stable system (Fig. 3d).

Following this, the characteristic features of the CaT-ME system were evaluated after copper peptides were loaded (named GHK-Cu/CaT-ME). The prepared GHK-Cu/CaT-ME was transparent and pale blue and had a glossy appearance (see Fig. 3e). CD spectroscopic investigations revealed no change in the structure of the copper peptides after being incorporated into the microemulsion system (Fig. 3f). Moreover, after storage at 25 °C (50 d) and centrifugation at 1500 rpm (30 min), GHK-Cu/CaT-ME did not demulsify (Fig. 3g), indicating good stability. FTIR spectra revealed no shift in the peaks of the copper peptides after being loaded onto the microemulsion system (Fig. 3h). These results showed that the GHK-Cu/CaT-ME system had adequate stability.

Safety is critical when designing carriers used for local drug delivery. Therefore, the effects of the developed system on cells were evaluated using a human fibroblast cell line (HFD). Figure S9 shows that each component only minimally inhibited cell proliferation at 0–800 µg/mL, indicating that the system was highly biocompatible. The calcein-AM/PI

staining assay results revealed few dead cells, with good survival rates of the cells in each treatment group, which is consistent with the results of cell proliferation experiments (Fig. 3i). These results demonstrate that GHK-Cu/CaT-ME had a good safety profile. Furthermore, we evaluated the biological function of GHK-Cu/CaT-ME to verify whether the carrier was suitable for delivering copper peptides. DPPH radical-scavenging experiments revealed that GHK-Cu/CaT-ME could effectively scavenge DPPH radicals, with a scavenging rate of almost 50 % at 800 µg/mL (Fig. 3j). In summary, the results indicated that the constructed GHK-Cu/CaT-ME system can adequately maintain the biological function of copper peptides.

2.4. Evaluation of the *in vitro* permeability of copper peptides

As the purpose of developing the GHK-Cu/CaT-ME system was to achieve localized delivery of copper peptides, we evaluated whether this system was effective in delivering loaded copper peptides via *in vitro* permeation experiments using scented pig skin [46–48]. The Franz diffusion cell method, which uses *ex vivo* skin with an intact stratum corneum, can effectively predict *in vivo* drug penetration (Fig. 4a). We evaluated the effects of PBS, L-carnitine, tartaric acid, CaT, and CaT-ME

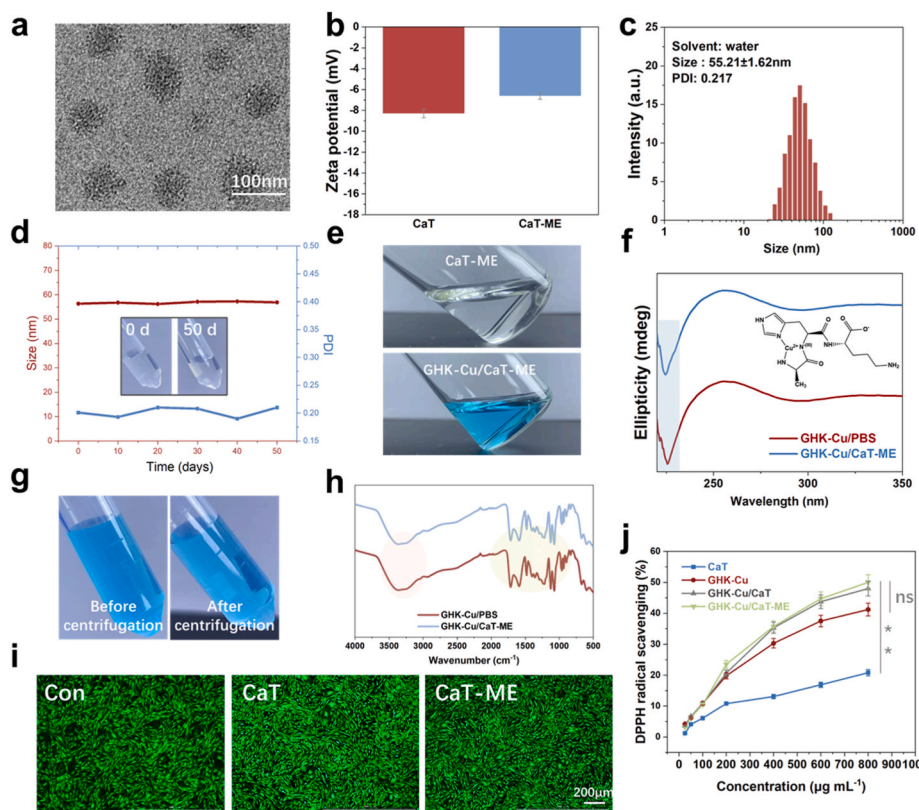


Fig. 3. Performance evaluation of the IL microemulsion. (a) TEM image of CaT-ME. Scale bar = 100 nm. (b) Zeta potentials of CaT and CaT-ME. (c) Size distribution of CaT-ME. (d) Size distribution and polydispersity index (PDI) of CaT-ME after 50 d of storage. The inset shows the changes before and after storage of CaT-ME (25 °C, 50 d). (e) Photographs of CaT-ME and GHK-Cu/CaT-ME. (f) Circular dichroism of copper peptides in different media. (g) Photographs of GHK-Cu/CaT-ME before and after centrifugation (1500 rpm, 30 min). (h) FTIR spectra of copper peptides in different media. (i) Cell proliferation after treatment with CaT and CaT-ME. Scale bar = 200 μm . (j) DPPH free radical-scavenging rate after treatment with different samples ($n = 3$). Results are provided as the mean \pm SD. * $p < 0.05$, ** $p < 0.01$.

as carriers on GHK-Cu permeation. Confocal microscopy (CLSM) images were obtained to assess the fluorescence intensity of each group after transdermal delivery. Among the different treatment groups, copper peptides were retained most in the skin when delivered using CaT-ME, resulting in a uniform fluorescence distribution with high intensity, which was 3.9-fold higher than that of the PBS group. The fluorescence intensity of the CaT group was 3.6-fold higher than that of the PBS group. In contrast, the L-carnitine-only and tartaric acid-only groups displayed weak fluorescence, and the fluorescence did not appear from the deeper layers of the porcine skin (Fig. 4b and c).

The cumulative permeation amount is a key parameter when evaluating drug delivery efficiency, which can be calculated using the following equation (1) (details of the parameters are given in the “Material and Methods” section):

$$Q_s (\mu\text{g cm}^{-2}) = C_{sm} \times \frac{V_s}{A_s} + \sum_{i=1}^{n-1} C_{Si} \times \frac{S}{A_s} \quad (1)$$

The calculated results (shown in Fig. 4d) revealed that the permeated amount of copper peptides was 2.65-fold higher after delivery using CaT than that using PBS, while it improved to 3.18-fold higher than that of the PBS group when using the CaT-ME system as the carrier. In contrast, using L-carnitine and tartaric acid as carriers did not significantly impact the permeation of copper peptides across the skin. Intradermal retention analyses indicated that copper peptides delivered via CaT and CaT-ME could reach deeper layers of the skin, whereas L-carnitine and tartaric acid could not assist in breaking through the stratum corneum barrier (Fig. 4e). These results indicate that both the CaT and CaT-ME systems can facilitate the local delivery of copper peptides, but the effect of CaT-ME is superior to that of CaT alone, possibly due to the synergistic pro-

permeation effect of IPM in the microemulsion system. However, L-carnitine and tartaric acid individually had no effect on the permeation of copper peptides, which further demonstrates the influence of the IL formulation on transdermal drug permeation. In addition, hematoxylin & eosin (H&E) staining indicated that there was no irritation or damage to the skin tissue after treatment with each group, confirming the safety of the developed system (Fig. 4f).

2.5. CaT-ME promoted hair growth in mice

The color of C57BL/6 mice skin correlates with the hair follicle cycle, and the growth cycle of the hair follicle can be determined based on changes in skin color of the mice [49,50]. When the skin is pink, the hair follicle is in the dormant phase, and when the skin turns gray, the hair follicle is in the anagen phase [51,52]. Therefore, we constructed a model of physical alopecia using C57BL/6 mice to evaluate the effects of the copper peptide emulsion system on hair growth (Fig. 5a). Initially, the PBS, CaT-ME, and CaT groups were evaluated via skin penetration experiments using FITC-labeled copper peptides (Fig. 5b). After 1 h of administration, the copper peptides from the CaT-ME and CaT groups had reached the hair follicle region, while those from the PBS group remained outside the stratum corneum. This trend is consistent with the results of the *in vitro* permeation assay. Subsequently, several groups (including a control group (Con) with saline, a positive drug group with FDA-approved 5 % minoxidil (Mi), and two experimental groups of CaT-ME and CaT (Fig. 5a)) were set up. During the treatment period, the CaT-ME-treated hair follicles entered the early stages of growth in as short as 6 d, exhibiting hyperpigmentation and hair regrowth. On the other hand, the CaT group and positive drug group displayed the same

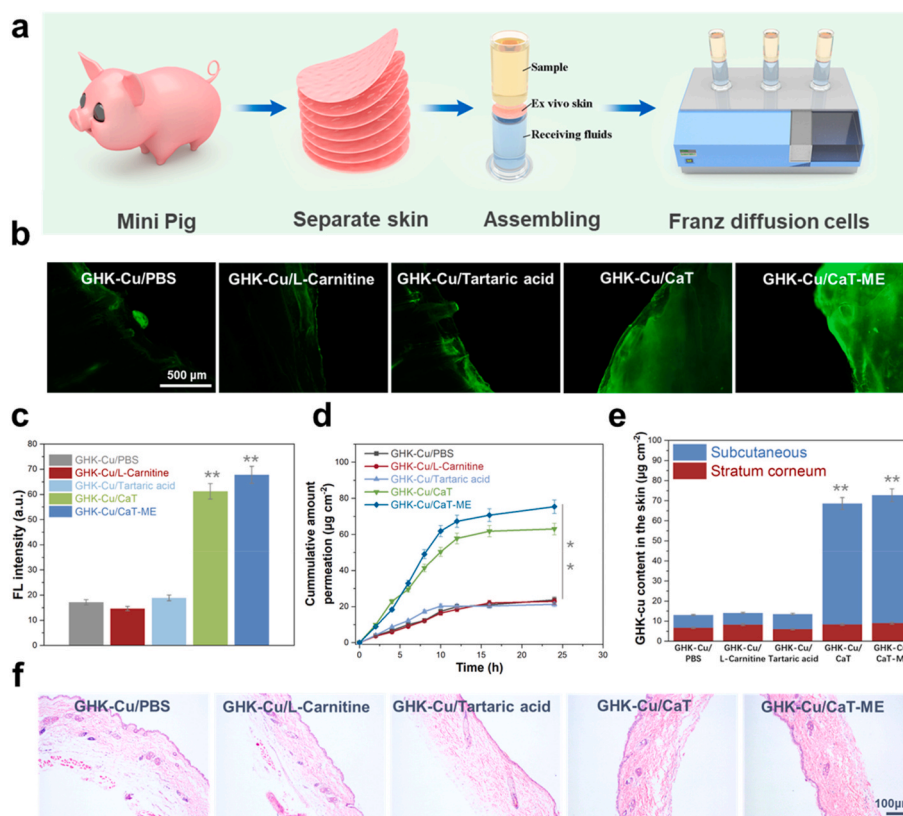


Fig. 4. Evaluation of the *in vitro* permeation of copper peptides. (a) Schematic of the *in vitro* permeation experiment. (b) CLSM images of copper peptides in porcine skin after delivery using PBS, L-carnitine, tartaric acid, CaT, and CaT-ME systems (scale bars = 500 µm) and (c) results of quantitative analysis (n = 3). (d) Cumulative penetration of copper peptides for different groups (n = 3). (e) Quantification of the copper peptides in the skin layers for different groups (n = 3). (f) Hematoxylin & eosin staining of the porcine skin after *in vitro* permeation experiments with different groups. Scale bar = 100 µm. Results are provided as the mean ± SD. *p < 0.05, **p < 0.01, ***p < 0.001.

effect after approximately 8 and 9 d, respectively. Calculations based on the hair cycle score confirmed that the CaT-ME and CaT groups had an earlier transition to hair growth (Fig. 5c).

At the end of 28 d, the number of hair follicles visualized by H&E staining was low in the control group, with the follicles were mostly located in the dermis. Using the same visual field as that of the positive drug group, mice in the CaT-ME and CaT groups exhibited significant increases in the number of hair follicles when compared to the control group, and the hair grew down to the subcutaneous tissue. Specifically, the hair density in the CaT-ME group was higher than those of the CaT and positive drug groups, which were comparable (Fig. 5e). In addition, mice in the CaT-ME and CaT groups had higher hair density than those in the Con and Mi groups (Fig. 5d). Masson staining revealed that the collagen fibers in the CaT-ME and CaT groups were more closely arranged and had better order than those of the control group. Collagen fibers are the basic structural units that impart toughness and resistance to tension to hair. Therefore, we speculate that treatment with CaT-ME and CaT may play a role in enhancing the toughness of hair and hair fixation (Fig. 5f). Hair pulling experiments also confirmed that the CaT-ME and CaT-induced neonatal hairs could not be easily stripped off with tape, similarly to the hair of wild-type mice. Furthermore, CaT-ME facilitated dermal thickening of the skin in mice, as assessed via H&E and Masson staining (Fig. 5e and f). Further, no significant differences were found between groups in terms of body weight, hair length, and hair weight (Table 1 and S1). No significant difference was observed in the body temperatures of mice from different groups before and after administration of their respective treatments (Table S2). Moreover, no injury to the skin was observed after treatment in each group. These results indicate that both the CaT-ME and CaT systems effectively promote the local absorption of copper peptides and have significant hair-

growth-promoting effects in mice. Their major mechanism of action is in shortening the time spent in the dormant phase and/or prolonging the anagen phase of hair follicles, leading to significantly increased hair density.

2.6. Mechanism underlying GHK-Cu/CaT-ME promoting hair growth

Hair follicle germination *in vivo* and *in vitro* is affected by various factors as it progresses through a complex and regulated cycle, which includes the anagen, catagen, and resting phases [53–55]. Therefore, we further explored the mechanism by which CaT-ME promotes hair growth. First, VEGF is produced in the blood vessels of hair follicles, stimulating hair growth *in vitro* and *in vivo* [56,57]. Further, hepatocyte growth factor (HGF) regulates the growth of hair papillae in hair follicle cells and induces hair growth by modulating the growth cycle [58,59]. As illustrated in Fig. 6a and b, all three treatments (minoxidil, CaT, and CaT-ME) could stimulate hair follicle cells to secrete VEGF and HGF, with the CaT group showing increased secretion of these factors compared with the minoxidil group. CaT-ME induced the most significant increase in VEGF and HGF secretion, which indicates that this system promoted growth factor expression and thus hair growth. In addition, as VEGF is a key stimulating factor in angiogenesis, its increased secretion implies that the developed CaT-ME system may contribute to the formation of vascular networks. Therefore, we examined CD31 expression; the immunofluorescence results revealed upregulated CD31 expression in the CaT and CaT-ME groups, suggesting that these two systems promoted local tissue angiogenesis (Fig. 6c).

Furthermore, as hormones can also affect hair growth [60], serum T and E2 levels in the mice were measured using ELISA kits, and the results indicated no significant variations in the T/E2 ratios in mice treated

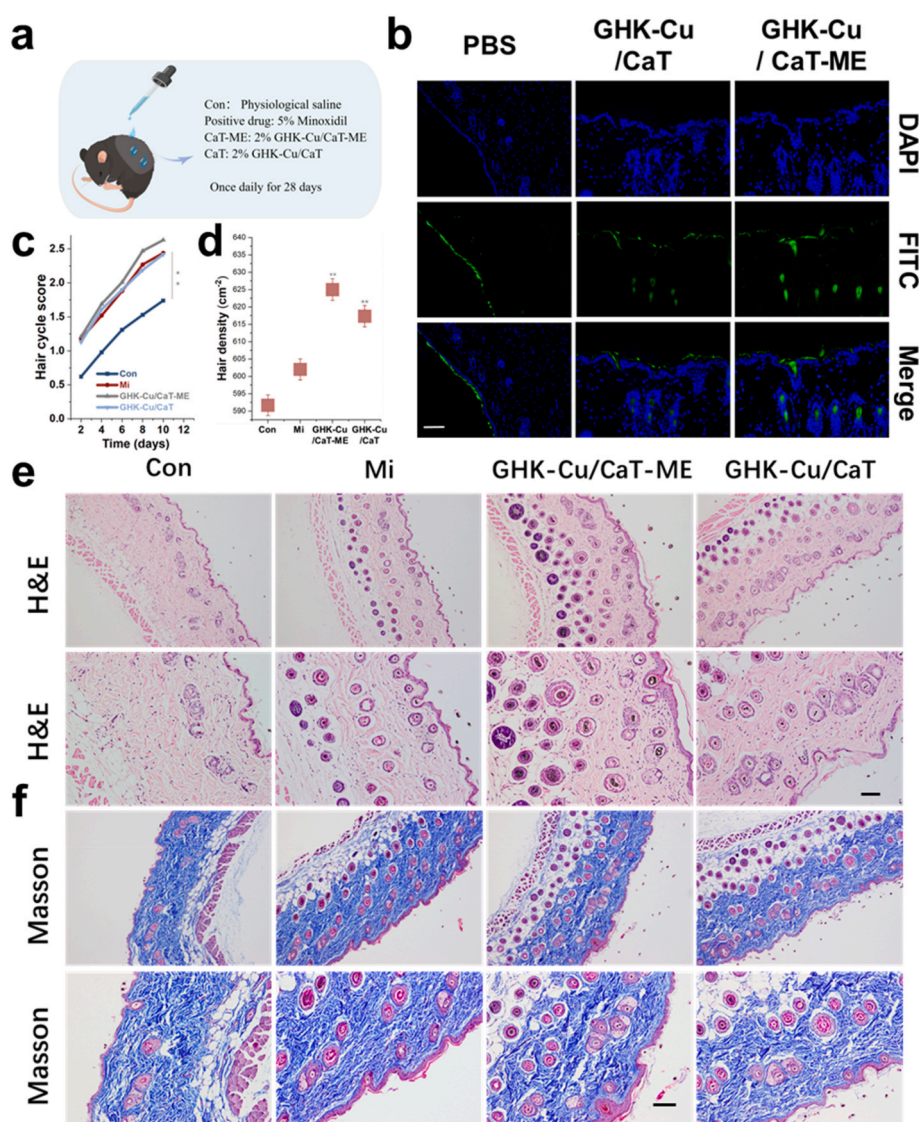


Fig. 5. Effect of GHK-Cu/CaT-ME *in vivo* experiments. (a) Schematic of hair loss treatment experiments in mice. (b) Representative images showing the intracutaneous penetration in mice in different groups after 1 h of treatment administration. Scale bar = 100 μ m. (c) Hair cycle score on day 10 post-depilation ($n = 3$). (d) Hair density of mice from different treatment groups ($n = 10$). (e and f) Hematoxylin & eosin (H&E) and Masson staining of the mice skin in different treatment groups. Scale bar = 100 μ m. Results are shown as the mean \pm SD. * $p < 0.05$, ** $p < 0.01$.

Table 1
Changes in body weight of mice in different treatment groups.

Groups	Body Weight (g)		
	Before mold-making	Pre-dose	Before-execution
Control	19.1	19.1	20.2
Minoxidil	18.9	18.9	20.1
GHK-Cu/CaT-ME	18.6	18.6	19.9
GHK-Cu/CaT	18.6	18.6	19.8

with CaT-ME or CaT, implying that these systems did not alter hormonal homeostasis in mice (Figure S10 and 11).

Additionally, various signaling pathways and related proteins play important roles in hair follicle regeneration, among which the Wnt signaling pathway is the classical example. β -catenin (a protein) is a key transcription factor that regulates hair follicle growth in this pathway [61,62]. Immunohistochemical results revealed an increase in the number of Ki67-positive cells in the CaT and CaT-ME groups when compared to that in the control group, reflecting the ability of the CaT and CaT-ME systems to facilitate skin cell proliferation. The increase in

β -catenin-positive markers indicates that CaT and CaT-ME promoted the expression of β -catenin (Fig. 6d). In addition, GSK3- β , which is located downstream of the Wnt signaling pathway, is also closely associated with the hair growth cycle [63,64]. Immunofluorescence staining suggested that the CaT and CaT-ME systems also promoted p -GSK3- β expression (Fig. 6g). These results suggest that the Wnt/ β -catenin pathway is activated by CaT and CaT-ME.

Finally, Ldha is a sugar-degrading enzyme that enhances hair follicle stem cell activation and plays a vital role in the hair growth cycle [65–67]. Western blotting was used to detect changes in Ldha expression, and the results revealed that Ldha expression was upregulated in skin follicles of mice in the experimental group when compared with mice in the control group, indicating that the CaT and CaT-ME systems promoted Ldha expression and accelerated the shift in the growth phase of hair follicles from the dormant to anagen phase, thus facilitating hair growth (Fig. 6e and f).

In summary, GHK-Cu/CaT-ME promotes hair growth by accelerating the hair follicle growth cycle. The main mechanisms include stimulating the expression of follicle-related growth factors, dilating scalp blood vessels and improving microcirculation, boosting the differentiation and

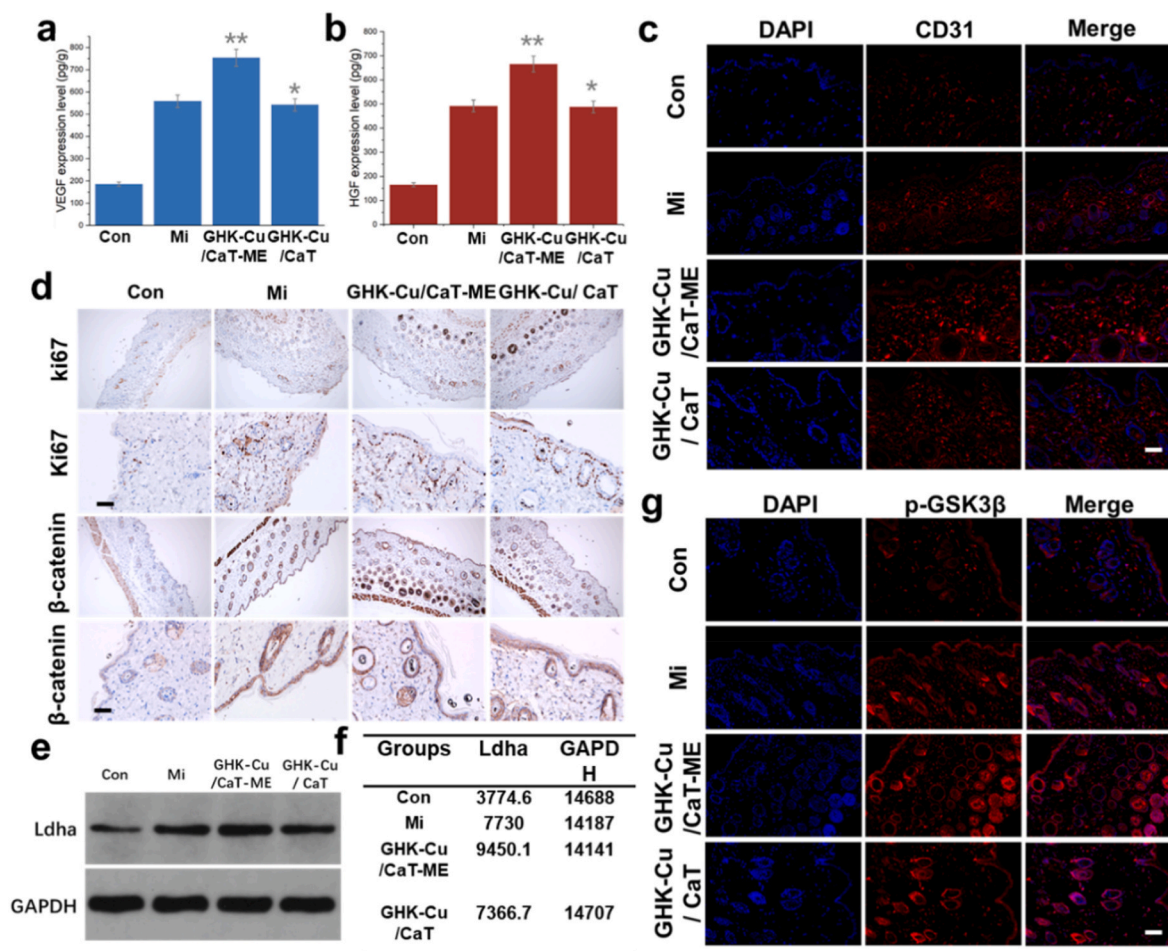


Fig. 6. Mechanism of GHK-Cu/CaT-ME in promoting hair growth. (a, b) VEGF and HGF expression levels in mice skin ($n = 3$). (c) Representative images of CD31 in the mice skin tissue after immunofluorescence staining (red: CD31; blue: DAPI). Scale bar = 50 μm . (d) Representative images of Ki67 and β -catenin in the mice skin tissue after immunohistochemical staining. Scale bar = 100 μm . (e, f) Qualitative and quantitative data of Ldha and GAPDH expression based on western blotting ($n = 3$). (g) Representative images of p -GSK3 β in the mice skin tissue after immunofluorescence staining (red: p -GSK3 β ; blue: DAPI). Scale bar = 50 μm . Results are presented as the mean \pm SD. * $p < 0.05$, ** $p < 0.01$.

proliferation of hair follicle epithelial cells, and activating the Wnt/ β -Catenin signaling pathway and its key proteins (Scheme 2).

3. Conclusion

Considering the challenges associated with the topical application of copper peptides for treating hair loss, this study focused on constructing a highly efficient transdermal delivery system. By combining theoretical calculations, material synthesis, and cellular and animal experiments, a bio-based IL microemulsion system was designed and developed for the localized delivery of copper peptides. Multi-dimensional analysis indicated that the proposed system has good stability and biological safety. The microemulsion system overcomes the adsorption issue of copper peptides and significantly improves their penetration efficiency. In animal experiments, it promoted hair growth, with excellent performance that surpassed that of commercially available minoxidil. Furthermore, we elucidated the key mechanisms and pathways by which this system promotes hair growth. Our study includes a comprehensive multidimensional analysis from the perspective of material design, synthesis and verification of the biological functions of the encapsulated drug, and mechanistic investigations. Our proposed system overcomes the difficulties associated with the topical administration of copper peptides and achieves efficient delivery in a localized and non-invasive manner. The microemulsion system is easy to prepare, cost-efficient, and has broad application prospects for topical drug delivery. Our study provides key

insights into the application of analogous active ingredients and has implications for cooperative use in cross-disciplinary fields.

4. Materials and methods

4.1. Materials

L-carnitine ($\geq 98\%$) and tartaric acid (99%) were purchased from Shanghai Macklin Biochemical Technology Co. (Shanghai, China). Copper peptides were purchased from Shenzhen Shinesky Biotechnology Co., Ltd. (Shenzhen, China). Dulbecco's modified Eagle's medium for cell culture, fetal bovine serum, and trypsin were purchased from Gibco (Grand Island, USA). CCK-8, DAPI, and DPPH kits, Calcein-AM/PI staining kit and paraformaldehyde (4%) were purchased from Biyuntian Biotechnology Co. (Shanghai, China). FITC-labeled copper peptides were purchased from Shanghai Chupeptide Biotechnology Co. (Shanghai, China), and skin fibroblasts (HFD) were purchased from Shanghai iCell Biotechnology Co. (Shanghai, China).

4.2. Synthesis of CaT

In this study, a series of CaT samples was prepared by mixing L-carnitine (cation) and tartaric acid (anion) at different molar ratios in water; In brief, the molecular weight of tartaric acid is 150.09, and the molecular weight of carnitine is 161.2. We initially designed the molar

ratio of tartaric acid and carnitine to be 1:1–3:1. According to the different molar ratios, the tartaric acid and L-carnitine powders were weighed separately and put into sample bottles at room temperature (25 °C). A small amount of water was added to the sample bottle and stirred until the liquid was clarified. The magnets were placed in a sample bottle and reacted in a 60 °C oil bath under nitrogen atmosphere for 24 h. The clarified liquid obtained was vortexed until the volume of the liquid stabilized and did not decrease any more. It was dried twice in a vacuum oven for 24 h. The end product obtained was CaT (Scheme 1).

4.3. Construction of ternary phase diagrams and preparation of microemulsions

The CaT-ME loaded with copper peptides was prepared by dissolving the drug in CaT used as the polar phase, and the drug-loaded sample is denoted as GHK-Cu/CaT-ME.

A pseudo-ternary phase diagram was obtained by titrating a mixture of IPM, Tween 80 and Span 20 with water at 25 °C. The ratio of Tween 80/Span 20 was varied as 1:1, 1:2, 2:1, 3:1, and 3:2. After the Tween 80/Span 20 ratio was optimized, the molar ratio of IPM to the Tween 80/Span 20 mixture was varied as 1:9, 2:8, 3:7, 4:6, 5:5, 6:4, 7:3, 8:2, and 9:1 to select the optimal ratio of IPM to the surfactant mixture. CaT was then added dropwise to the mixture (IPM/Tween80/Span20) under magnetic stirring until the resulting mixture changed from clear to turbid to clear. The amount of CaT added at the critical point was recorded and the proportion of each component was recorded. The emulsions formed in the single-phase and two-phase regions were clear and turbid, respectively. Water-in-oil microemulsions can be prepared by replacing CaT with water as described above.

4.4. Characterization of CaT, CaT-ME and GHK-cu/cat-me

¹H NMR spectra of CaT samples dissolved in CDCl₃ were recorded with a Bruker Avance spectrometer at 400 MHz. The FTIR spectra of the CaT and CaT-ME samples were recorded using a Thermo Scientific Nicolet iS 50 FTIR spectrometer in the attenuated total reflection mode. TGA was performed using a PerkinElmer-TGA 8000 instrument (Shanghai, China) in a nitrogen gas stream at a heating rate of 10 °C/min in the temperature range of 50–60 °C. DSC was performed in a nitrogen atmosphere using a thermal analyzer, and the system was cooled using liquid nitrogen at the rate of 10 °C/min (Mettler Toledo DSC3, Switzerland).

4.5. Cell experiments

4.5.1. In vitro cytotoxicity assay

Cells (HFD) in the logarithmic growth phase were seeded into 96-well cell culture plates (6000 cells/well) and incubated overnight at 37 °C and 5 % CO₂. Different concentrations of samples to be tested were added according to the experimental design. Then, 10 μL of the CCK-8 solution was added to each well after incubation at 37 °C for a fixed time and the samples were incubated further for 1–6 h. The absorbance was measured at 450 nm using an enzyme marker (BioTek, Gen 5), and the growth rate of cells was calculated as follows:

$$\text{Cell viability (\%)} = \frac{A_{\text{test}} - A_{\text{blank}}}{A_{\text{control}} - A_{\text{blank}}} \times 100\%$$

where A_{blank} is the absorbance of the wells without cells, and A_{control} and A_{test} are the absorbances of the control and treated cells, respectively.

4.5.2. Calcein-AM/PI cell staining

Live/dead cells were analyzed by staining with PBS (100 μL) containing calcein-AM reagent (10 μL) and propidium iodide stock solution (10 μL). The stained cells were incubated at 37 °C for 30 min and observed with a CLSM.

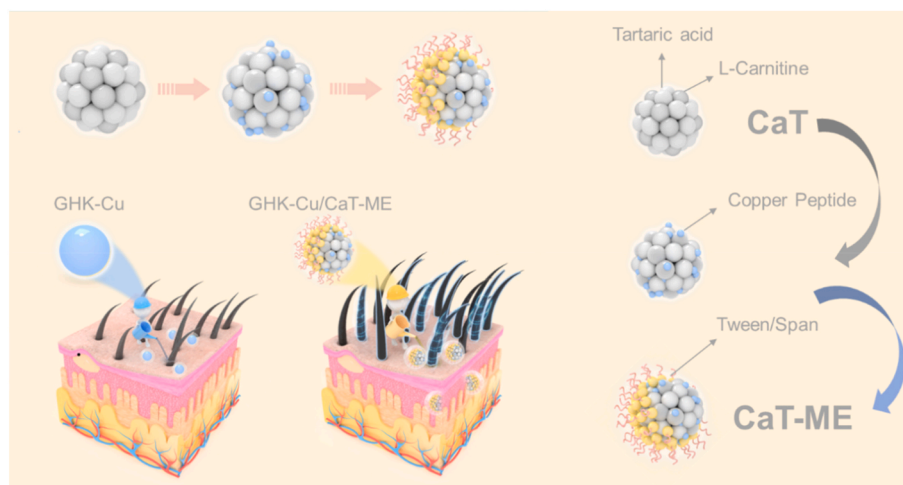
4.6. Transdermal diffusion test in vitro

4.6.1. Skin preparation

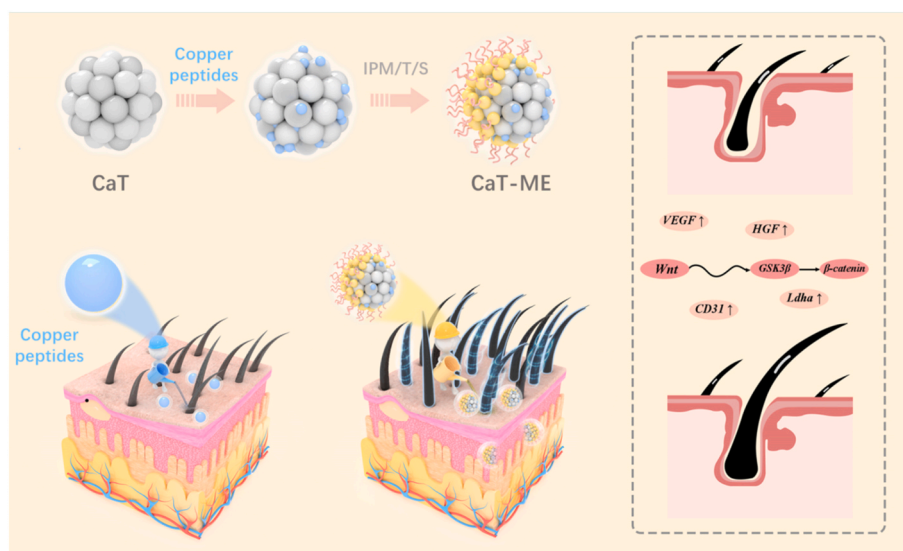
First, the skin was promptly peeled off the euthanized miniature scent pig. Then, the long hairs on the skin were carefully removed using an electric razor, and the remaining hairs were gently scraped off with a small knife. The remaining fat and mucosal tissues in the skin tissue were cleaned, coated with normal saline, wrapped in plastic wrap, and stored in a 4 °C refrigerator.

4.6.2. In vitro skin penetration test

Transdermal experiments were performed using Franz diffusion cells. Fresh porcine skin was fixed between the diffusion cell and receiver cell with the dermis facing the receiver cell. First, magnets were placed in the receiver cell, and it was filled with 0.01 M PBS. The test samples were loaded into the diffusion cell and wrapped with cling film to prevent solvent evaporation. The experiment was performed at 32 °C and 300 rpm. A 2 mL volume of the sample (V_0) was retrieved from the receiver cell after different time intervals, and the cell was supplemented with 2 mL of fresh PBS. The cumulative permeability was determined through high-performance liquid chromatography (HPLC); it was calculated using the following equation:



Scheme 1. Schematic diagram of CaT-ME formation.



Scheme 2. Schematic diagram of GHK-Cu/CaT-ME system construction and its mechanism of action.

$$Q_s (\mu\text{g cm}^{-2}) = C_{sn} \times \frac{V_s}{A_s} + \sum_{i=1}^{n-1} C_{Si} \times \frac{S}{A_s}$$

where, Q_s is the cumulative drug permeation per unit area ($\mu\text{g}\cdot\text{cm}^{-2}$), C_{sn} is the drug concentration measured in the receptor fluid at n sampling intervals ($\mu\text{g}\cdot\text{m}\cdot\text{L}^{-1}$), V_s is the volume of the receptor pool (13 mL), $\sum_{i=1}^{n-1} C_{Si}$ is the cumulative drug concentration in the receptor fluid, S is the sampling volume (2 mL), and A_s is the effective diffusion area (1.0 cm^2). Finally, the skin used for transdermal delivery was collected and washed repeatedly with PBS. A portion of the skin was fixed with 4 % paraformaldehyde and embedded in paraffin wax for immunohistochemical staining.

4.6.3. Measurement of the drug content in porcine skin

After the experiment, the porcine skin was cleaned with PBS. The stratum corneum was obtained by repeatedly applying 10 strips of clear adhesive, and the remaining skin was cut into effective diffusion zones and sliced further to obtain the subcutaneous tissue. The different stratified skin layers were suspended in methanol and the copper peptides were extracted by ultrasonication. After centrifugation at 1300 g for 15 min, the supernatant was collected by filtration through a $0.45 \mu\text{m}$ filtration membrane. Finally, the drug content in each skin layer was determined by HPLC.

4.6.4. Chromatographic quantification (HPLC) analysis

A C18 column (ZORBAX Eclipse) in HPLC-UV (Agilent 1100) was used for quantitative determination of copper peptide concentrations. The mobile phase consisted of (A) water, (B) methanol, and (C) 0.1 % aqueous trifluoroacetic acid. The detection wavelength was 220 nm and the injection volume was $5 \mu\text{L}$; the column temperature was set at $25 \text{ }^\circ\text{C}$; the flow rate was $1.0 \text{ mL}/\text{min}$.

The gradient elution sequence is shown in the table below.

Time (minutes)	A%	B%	C%
0	0	5	95
10	0	5	95
10.01	90	10	0
15	90	10	0
24	0	100	0
34	0	100	0
34.01	95	5	0
35	95	5	0
35.01	0	5	95
45	0	5	95

4.7. Animal experiments

C57BL/6 J mice purchased from three Gorges University Animal Center (Yichang, Hubei, China) was used in this study. The license number is SCXK(Er) 2017–0012. All animal experiments were performed in accordance with animal research protocols approved by the Animal Care and Use Committee of Peking University. In the *in vivo* experiments, mice were shaved (Back: $2 \times 3 \text{ cm}$ [2]) on the 50th day from birth and the depilated areas were coated with saline, 5 % minoxidil, CaT containing 2 % copper peptides, and CaT-ME containing 2 % copper peptides daily after shaving, with 6 mice per group. Application twice daily for 21 days, followed by fasting for 12 h and then execution of the mice for sampling. Temperature was measured daily before and after administration to evaluate the body temperature changes of the mice. Measurement time 20 min before dosing, 0 min, 20 min, 60 min, 120 min after dosing. The body weight of the mice was measured at specific times. Temporal profiles of hair phenotypic transformation were obtained through real-time observation of hair regeneration in the mice. Fixed size skin pieces were peeled and weighed, and weighed again after hair removal, and three pieces were taken for each group for repeated measurements to obtain the weight of newly grown hairs in the mice.

4.8. DFT calculations

Gaussian 09 software and B3LYP-D3 functions were used to optimize the molecular structure. The frequency analysis and electrostatic potential analyses were performed using 6–311 G** basis set 58. RDG analysis was conducted using Multiwfn and Winvmd programs.

4.9. Statistical analysis

The results are presented as mean \pm standard deviation. One-way analysis of variance was used to determine the significance of differences. Statistical significance is set as ns: no statistical difference, *: $p < 0.05$, **: $p < 0.01$, ***: $p \leq 0.001$.

Data availability

All the relevant data are available from the corresponding authors

upon reasonable request.

CRedit authorship contribution statement

Tianqi Liu: Conceptualization, Data curation, Formal analysis, Investigation, Writing – original draft. **Ying Liu:** Formal analysis, Writing – review & editing. **Xiaoyu Zhao:** Investigation, Visualization. **Liguo Zhang:** Writing – review & editing. **Wei Wang:** Investigation. **De Bai:** Formal analysis. **Ya Liao:** Formal analysis. **Zhenyuan Wang:** Data curation, Methodology, Resources. **Mi Wang:** Validation, Writing – review & editing. **Jiaheng Zhang:** Conceptualization, Funding acquisition, Supervision, Project administration, Writing – review & editing.

Declaration of competing interest

The authors declare no conflict of interest.

Acknowledgments

Tianqi Liu, Ying Liu, Xiaoyu Zhao contributed equally to this work. Support was received from the National Natural Science Foundation of China (21703218), Shenzhen Science and Technology Innovation Commission (JCYJ20180507183907224, KQTD20170809110344233), and Shenzhen Economic, Trade and Information Commission through the Graphene Manufacturing Innovation Center (201901161514). The Guangdong Provincial Covid-19 Pandemic Control Research Fund (2020KZDZX1220).

Appendix A. Supplementary data

Supplementary data to this article can be found online at <https://doi.org/10.1016/j.bioactmat.2023.10.002>

Supporting Information

Synthesis and characterization of LM and LM-ME and other related experiments.

References

- [1] L. Li, R.M. Hoffman, The feasibility of targeted selective gene therapy of the hair follicle, *Nat. Med.* 1 (7) (1995) 705–706, <https://doi.org/10.1038/nm0795-705>.
- [2] S. Salim, K. Kamalasanan, Controlled drug delivery for alopecia: a review, *J. Contr. Release* 325 (2020) 84–99, <https://doi.org/10.1016/j.jconrel.2020.06.019>.
- [3] Y. Shi, J. Zhao, H. Li, M. Yu, W. Zhang, D. Qin, K. Qiu, X. Chen, M. Kong, A drug-free, hair follicle cycling regulatable, separable, antibacterial microneedle patch for hair regeneration therapy, *Adv. Healthcare Mater.* 11 (19) (2022), 2200908, <https://doi.org/10.1002/adhm.202200908>.
- [4] R. Wang, T. Zhong, Q. Bian, S. Zhang, X. Ma, L. Li, Y. Xu, Y. Gu, A. Yuan, W. Hu, et al., PROTAC degraders of androgen receptor-integrated dissolving microneedles for androgenetic alopecia and recrudescence treatment via single topical administration, *Small Methods* 7 (1) (2023), 2201293, <https://doi.org/10.1002/smt.202201293>.
- [5] C.A.B. Jahoda, K.A. Horne, R.F. Oliver, Induction of hair growth by implantation of cultured dermal papilla cells, *Nature* 311 (5986) (1984) 560–562, <https://doi.org/10.1038/311560a0>.
- [6] S. Ji, Z. Zhu, X. Sun, X. Fu, Functional hair follicle regeneration: an updated review, *Signal Transduct. Targeted Ther.* 6 (1) (2021) 66, <https://doi.org/10.1038/s41392-020-00441-y>.
- [7] S.D. Bhinge, M.A. Bhutkar, D.S. Randive, G.H. Wadkar, S.S. Todkar, A.S. Savali, H. R. Chittapurkar, Screening of hair growth promoting activity of Punica granatum L. (pomegranate) leaves extracts and its potential to exhibit antidandruff and anti-lice effect, *Heliyon* 7 (4) (2021), <https://doi.org/10.1016/j.heliyon.2021.e06903>.
- [8] M. Randolph, A. Tosti, Oral minoxidil treatment for hair loss: a review of efficacy and safety, *J. Am. Acad. Dermatol.* 84 (3) (2021) 737–746, <https://doi.org/10.1016/j.jaad.2020.06.1009>.
- [9] J.R. Stoehr, J.N. Choi, M. Colavincenzo, S. Vanderweil, Off-label use of topical minoxidil in alopecia: a review, *Am. J. Clin. Dermatol.* 20 (2) (2019) 237–250, <https://doi.org/10.1007/s40257-018-0409-y>.
- [10] Q. Xiao, L. Wang, S. Supekhar, T. Shen, H. Liu, F. Ye, J. Huang, H. Fan, Z. Wei, C. Zhang, Structure of human steroid 5 α -reductase 2 with the anti-androgen drug finasteride, *Nat. Commun.* 11 (1) (2020) 5430, <https://doi.org/10.1038/s41467-020-19249-z>.
- [11] S.L. Gray, T.P. Semla, Post-finasteride syndrome, *BMJ* 366 (2019) l5047, <https://doi.org/10.1136/bmj.l5047>.
- [12] D.-D. Nguyen, M. Marchese, E.B. Cone, M. Paciotti, S. Basaria, N. Bhojani, Q.-D. Trinh, Investigation of suicidality and psychological adverse events in patients treated with finasteride, *JAMA Dermatol.* 157 (1) (2021) 35–42, <https://doi.org/10.1001/jamadermatol.2020.3385>.
- [13] J.Y. Kim, J. Ohn, J.-S. Yoon, B.M. Kang, M. Park, S. Kim, W. Lee, S. Hwang, J.-I. Kim, K.H. Kim, et al., Priming mobilization of hair follicle stem cells triggers permanent loss of regeneration after alkylating chemotherapy, *Nat. Commun.* 10 (1) (2019) 3694, <https://doi.org/10.1038/s41467-019-11665-0>.
- [14] M.J. Kim, K.-Y. Seong, D.S. Kim, J.S. Jeong, S.Y. Kim, S. Lee, S.Y. Yang, B.-S. An, Minoxidil-loaded hyaluronic acid dissolving microneedles to alleviate hair loss in an alopecia animal model, *Acta Biomater.* 143 (2022) 189–202, <https://doi.org/10.1016/j.actbio.2022.02.011>.
- [15] M. Pereira-Silva, A.M. Martins, I. Sousa-Oliveira, H.M. Ribeiro, F. Veiga, J. Marto, A.C. Paiva-Santos, Nanomaterials in hair care and treatment, *Acta Biomater.* 142 (2022) 14–35, <https://doi.org/10.1016/j.actbio.2022.02.025>.
- [16] M. Zhou, X. Wu, J. Luo, G. Yang, Y. Lu, S. Lin, F. Jiang, W. Zhang, X. Jiang, Copper peptide-incorporated 3D-printed silk-based scaffolds promote vascularized bone regeneration, *Chem. Eng. J.* 422 (2021), 130147, <https://doi.org/10.1016/j.cej.2021.130147>.
- [17] Y. Li, X. Cai, Z. Wang, Y. Han, C. Ren, L. Yang, Z. Wang, G. Mu, H. Jia, J. Liu, et al., Bio-inspired supramolecular metalloprotein hydrogel promotes recovery from cutaneous wound, *Chem. Eng. J.* 455 (2023), 140848, <https://doi.org/10.1016/j.cej.2022.140848>.
- [18] L. Pickart, J.M. Vasquez-Soltero, A. Margolina, GHK and DNA: resetting the human genome to health, *BioMed Res. Int.* 2014 (2014), 151479, <https://doi.org/10.1155/2014/151479>.
- [19] J. Hwang, K.L. Kiick, M.O. Sullivan, VEGF-encoding, gene-activated collagen-based matrices promote blood vessel formation and improved wound repair, *ACS Appl. Mater. Interfaces* 15 (13) (2023) 16434–16447, <https://doi.org/10.1021/acsami.2c23022>.
- [20] M. Elsnar, New role for VEGF, *Nat. Biotechnol.* 29 (12) (2011), <https://doi.org/10.1038/nbt.2073>, 1101–1101.
- [21] S. Lee, T.T. Chen, C.L. Barber, M.C. Jordan, J. Murdock, S. Desai, N. Ferrara, A. Nagy, K.P. Roos, M.L. Iruela-Arispe, Autocrine VEGF signaling is required for vascular homeostasis, *Cell* 130 (4) (2007) 691–703, <https://doi.org/10.1016/j.cell.2007.06.054>.
- [22] H. Heloterä, K. Alitalo, The VEGF family, the inside story, *Cell* 130 (4) (2007) 591–592, <https://doi.org/10.1016/j.cell.2007.08.012>.
- [23] Z. Liu, X. Hu, Y. Liang, J. Yu, H. Li, M.N. Shokhirev, Y. Zheng, Glucocorticoid signaling and regulatory T cells cooperate to maintain the hair-follicle stem-cell niche, *Nat. Immunol.* 23 (7) (2022) 1086–1097, <https://doi.org/10.1038/s41590-022-01244-9>.
- [24] K. Foitzik, G. Lindner, S. Mueller-Roever, M. Maurer, N. Botchkareva, V. Botchkarev, B. Handjiski, M. Metz, T. Hibino, T. Soma, et al., Control of murine hair follicle regression (catagen) by TGF- β 1 in vivo, *Faseb. J.* 14 (5) (2000) 752–760, <https://doi.org/10.1096/fasebj.14.5.752>.
- [25] J. Lee, C.C. Rabbani, H. Gao, M.R. Steinhart, B.M. Woodruff, Z.E. Pflum, A. Kim, S. Heller, Y. Liu, T.Z. Shipchandler, et al., Hair-bearing human skin generated entirely from pluripotent stem cells, *Nature* 582 (7812) (2020) 399–404, <https://doi.org/10.1038/s41586-020-2352-3>.
- [26] H.M. Sowden, R.O.S. Karoo, D.J. Tobin, Transforming growth factor- β receptor II is preferentially expressed in the companion layer of the human anagen hair follicle, *Br. J. Dermatol.* 157 (1) (2007) 161–164, <https://doi.org/10.1111/j.1365-2133.2007.07925.x>.
- [27] Z. Liu, J. Huang, D. Kang, Y. Zhou, L. Du, Q. Qu, J. Wang, L. Wen, D. Fu, Z. Hu, et al., Microenvironmental reprogramming of human dermal papilla cells for hair follicle tissue engineering, *Acta Biomater.* 165 (2023) 31–49, <https://doi.org/10.1016/j.actbio.2022.11.004>.
- [28] Y. Liu, C.F. Guerrero-Juarez, F. Xiao, N.U. Shettigar, R. Ramos, C.-H. Kuan, Y.-C. Lin, L. de Jesus Martinez Lomeli, J.M. Park, J.W. Oh, et al., Hedgehog signaling reprograms hair follicle niche fibroblasts to a hyper-activated state, *Dev. Cell* 57 (14) (2022), <https://doi.org/10.1016/j.devcel.2022.06.005>, 1758–1775.e1757.
- [29] T. Liu, L. Zhang, B. Lu, D. Li, Y. Bo, W. Wang, Z. Wang, Y. Liao, J. Zhan, C. Wu, et al., Noninvasive and efficient peptide delivery by a novel biocompatible ionic liquid, *ACS Sustain. Chem. Eng.* 10 (50) (2022) 16611–16623, <https://doi.org/10.1021/acssuschemeng.2c04422>.
- [30] S. Meiners, O. Eickelberg, Next-generation personalized drug discovery: the tripeptide GHK hits center stage in chronic obstructive pulmonary disease, *Genome Med.* 4 (8) (2012) 70, <https://doi.org/10.1186/gm371>.
- [31] L.-W. Tian, D. Luo, D. Chen, H. Zhou, X.-C. Zhang, X.-L. Yang, Y.-L. Wang, W. Liu, Co-delivery of bioactive peptides by nanoliposomes for promotion of hair growth, *J. Drug Deliv. Sci. Technol.* 72 (2022), 103381, <https://doi.org/10.1016/j.jddst.2022.103381>.
- [32] E. Ayhan, Z. Tuna, C. Oksuz, Getting better results in flexor tendon surgery and therapy, *Plast Reconstr Surg. Glob. Open* 9 (2) (2021), e3432, <https://doi.org/10.1097/gox.0000000000003432> From NLM.
- [33] J.D. Campbell, J.E. McDonough, J.E. Zeskind, T.L. Hackett, D.V. Pechkovsky, C.-A. Brandsma, M. Suzuki, J.V. Gosselink, G. Liu, Y.O. Alekseyev, et al., A gene expression signature of emphysema-related lung destruction and its reversal by the tripeptide GHK, *Genome Med.* 4 (8) (2012) 67, <https://doi.org/10.1186/gm367>.
- [34] S. Jose, M.L. Hughbanks, B.Y.K. Binder, G.C. Ingavle, J.K. Leach, Enhanced trophic factor secretion by mesenchymal stem/stromal cells with Glycine-Histidine-Lysine (GHK)-modified alginate hydrogels, *Acta Biomater.* 10 (5) (2014) 1955–1964, <https://doi.org/10.1016/j.actbio.2014.01.020>.

- [35] K.R. Jadhav, I.M. Shaikh, K.W. Ambade, V.J. Kadam, Applications of microemulsion based drug delivery system, *Curr. Drug Deliv.* 3 (3) (2006) 267–273, [10.2174/15672010677731118](https://doi.org/10.2174/15672010677731118) From *NLM*.
- [36] Z. Laron, B.E. Halberstadt, Total and l(+)- tartaric acid inhibited rat serum acid phosphatase, *Nature* 187 (4731) (1960) 67–68, <https://doi.org/10.1038/187067a0>.
- [37] Zhang, F.; Lv, M.; Wang, S.; Li, M.; Wang, Y.; Hu, C.; Hu, W.; Wang, X.; Wang, X.; Liu, Z.; et al. Ultrasound-triggered biomimetic ultrashort peptide nanofiber hydrogels promote bone regeneration by modulating macrophage and the osteogenic immune microenvironment. *Bioact. Mater.* 2024, 31, 231–246. DOI: 10.1016/j.bioactmat.2023.08.008.
- [38] M. Bonomini, A. Pandolfi, L. Di Liberato, S. Di Silvestre, Y. Cnops, P. Di Tomo, M. D'Arezzo, M.P. Monaco, A. Giardinelli, N. Di Pietro, et al., Span class small span Carnitine is an osmotic agent suitable for peritoneal dialysis, *Kidney Int.* 80 (6) (2011) 645–654, <https://doi.org/10.1038/ki.2011.117>.
- [39] R.A. Cruciani, E. Dvorkin, P. Homel, B. Culliney, S. Malamud, S. Fleishman, J. Lapin, P. Lesage, R. Portenoy, N.V. Cruciani-Esteban, L-carnitine supplementation in cancer patients with fatigue and carnitine deficiency, *J. Clin. Oncol.* 22 (14) (2004), <https://doi.org/10.1200/jco.2004.22.90140.8025>, 8025–8025.
- [40] L.-Y. Li, S.M. Limbu, Q. Ma, L.-Q. Chen, M.-L. Zhang, Z.-Y. Du, The metabolic regulation of dietary L-carnitine in aquaculture nutrition: present status and future research strategies, *Rev. Aquacult.* 11 (4) (2019) 1228–1257, [10.1111/raq.12289](https://doi.org/10.1111/raq.12289).
- [41] K. Foitzik, E. Hoting, T. Förster, P. Pertile, R. Paus, L-Carnitine–L-tartrate promotes human hair growth in vitro, *Exp. Dermatol.* 16 (11) (2007) 936–945, <https://doi.org/10.1111/j.1600-0625.2007.00611.x>.
- [42] N. Kapate, J.R. Clegg, S. Mitragotri, Non-spherical micro- and nanoparticles for drug delivery: progress over 15 years, *Adv. Drug Deliv. Rev.* 177 (2021), 113807, <https://doi.org/10.1016/j.addr.2021.05.017>.
- [43] S. Venkataraman, J.L. Hedrick, Z.Y. Ong, C. Yang, P.L.R. Ee, P.T. Hammond, Y. Yang, The effects of polymeric nanostructure shape on drug delivery, *Adv. Drug Deliv. Rev.* 63 (14) (2011) 1228–1246, <https://doi.org/10.1016/j.addr.2011.06.016>.
- [44] B. Lu, Y. Bo, M. Yi, Z. Wang, J. Zhang, Z. Zhu, Y. Zhao, J. Zhang, Enhancing the solubility and transdermal delivery of drugs using ionic liquid-in-oil microemulsions, *Adv. Funct. Mater.* 31 (34) (2021), 2102794, <https://doi.org/10.1002/adfm.202102794>.
- [45] M.-B. Cheng, J.-C. Wang, Y.-H. Li, X.-Y. Liu, X. Zhang, D.-W. Chen, S.-F. Zhou, Q. Zhang, Characterization of water-in-oil microemulsion for oral delivery of earthworm fibrinolytic enzyme, *J. Contr. Release* 129 (1) (2008) 41–48, <https://doi.org/10.1016/j.jconrel.2008.03.018>.
- [46] Q.M. Qi, M. Duffy, A.M. Curreri, J.P.R. Balkaran, E.E.L. Tanner, S. Mitragotri, Comparison of ionic liquids and chemical permeation enhancers for transdermal drug delivery, *Adv. Funct. Mater.* 30 (45) (2020), 2004257, <https://doi.org/10.1002/adfm.202004257>.
- [47] E.E.L. Tanner, A.M. Curreri, J.P.R. Balkaran, N.C. Selig-Wober, A.B. Yang, C. Kendig, M.P. Fluhr, N. Kim, S. Mitragotri, Design principles of ionic liquids for transdermal drug delivery, *Adv. Mater.* 31 (27) (2019), 1901103, <https://doi.org/10.1002/adma.201901103>.
- [48] T. Jiang, G. Xu, G. Chen, Y. Zheng, B. He, Z. Gu, Progress in transdermal drug delivery systems for cancer therapy, *Nano Res.* 13 (7) (2020) 1810–1824, <https://doi.org/10.1007/s12274-020-2664-5>.
- [49] G. Yang, Q. Chen, D. Wen, Z. Chen, J. Wang, G. Chen, Z. Wang, X. Zhang, Y. Zhang, Q. Hu, et al., A therapeutic microneedle patch made from hair-derived keratin for promoting hair regrowth, *ACS Nano* 13 (4) (2019) 4354–4360, <https://doi.org/10.1021/acsnano.8b09573>.
- [50] S.M. Cattaneo, H. Quastler, F.G. Sherman, Proliferative cycle in the growing hair follicle of the mouse, *Nature* 190 (4779) (1961) 923–924, <https://doi.org/10.1038/190923a0>.
- [51] Z. Zhang, W. Li, D. Chang, Z. Wei, E. Wang, J. Yu, Y. Xu, Y. Que, Y. Chen, C. Fan, et al., A combination therapy for androgenic alopecia based on quercetin and zinc/copper dual-doped mesoporous silica nanocomposite microneedle patch, *Bioact. Mater.* 24 (2023) 81–95, <https://doi.org/10.1016/j.bioactmat.2022.12.007>.
- [52] R.R. Chavan, S.D. Bhinghe, M.A. Bhutkar, D.S. Randive, G.H. Wadkar, S.S. Todkar, In vivo and in vitro hair growth-promoting effect of silver and iron nanoparticles synthesized via *Blumea eriantha* DC plant extract, *J. Cosmet. Dermatol.* 20 (4) (2021) 1283–1297, <https://doi.org/10.1111/jocd.13713>.
- [53] K. Davies, Hair apparent, *Nature* 391 (6667) (1998) 537–538, <https://doi.org/10.1038/35264>.
- [54] L. Chessum, M.S. Matern, M.C. Kelly, S.L. Johnson, Y. Ogawa, B. Milton, M. McMurray, E.C. Driver, A. Parker, Y. Song, et al., Helios is a key transcriptional regulator of outer hair cell maturation, *Nature* 563 (7733) (2018) 696–700, <https://doi.org/10.1038/s41586-018-0728-4>.
- [55] S.D. Bhinghe, M.A. Bhutkar, D.S. Randive, G.H. Wadkar, S.S. Todkar, A.S. Savali, H. R. Chittapurkar, Screening of hair growth promoting activity of *Punica granatum L.* (pomegranate) leaves extracts and its potential to exhibit antidandruff and anti-lice effect, *Heliyon* 7 (4) (2021), e06903, <https://doi.org/10.1016/j.heliyon.2021.e06903>.
- [56] R. Morita, N. Sanzen, H. Sasaki, T. Hayashi, M. Umeda, M. Yoshimura, T. Yamamoto, T. Shibata, T. Abe, H. Kiyonari, et al., Tracing the origin of hair follicle stem cells, *Nature* 594 (7864) (2021) 547–552, <https://doi.org/10.1038/s41586-021-03638-5>.
- [57] M. Ehrbar, S.M. Zeisberger, G.P. Raeber, J.A. Hubbell, C. Schnell, A.H. Zisch, The role of actively released fibrin-conjugated VEGF for VEGF receptor 2 gene activation and the enhancement of angiogenesis, *Biomaterials* 29 (11) (2008) 1720–1729, <https://doi.org/10.1016/j.biomaterials.2007.12.002>.
- [58] S.D. Bhinghe, N.R. Jadhav, D.S. Randive, M.A. Bhutkar, R. Chavan, B.V. Kumbhar, Isolation and identification of hair growth potential fraction from active plant extract of *Blumea eriantha* DC grown in Western Ghat of India: in silico study, *J. Ayurveda Integr. Med.* 13 (2) (2022), 100542, <https://doi.org/10.1016/j.jaim.2022.100542>.
- [59] A. Savali, H. Chitapurkar, S. Bhinghe, Evaluation of hair growth promoting activity of *Musa paradisiaca* unripe fruit extract, *J. Nat. Pharmaceu.* 2 (3) (2011) 120, <https://doi.org/10.4103/2229-5119.86257>.
- [60] J.-Y. Ryu, E.-J. Won, H.A.R. Lee, J.H. Kim, E. Hui, H.P. Kim, T.-J. Yoon, Ultrasound-activated particles as CRISPR/Cas9 delivery system for androgenic alopecia therapy, *Biomaterials* 232 (2020), 119736, <https://doi.org/10.1016/j.biomaterials.2019.119736>.
- [61] M. Ito, Z. Yang, T. Andl, C. Cui, N. Kim, S.E. Millar, G. Cotsarelis, Wnt-dependent de novo hair follicle regeneration in adult mouse skin after wounding, *Nature* 447 (7142) (2007) 316–320, <https://doi.org/10.1038/nature05766>.
- [62] S. Fakhraei Lahiji, S.H. Seo, S. Kim, M. Dangel, J. Shim, C.G. Li, Y. Ma, C. Lee, G. Kang, H. Yang, et al., Transcutaneous implantation of valproic acid-encapsulated dissolving microneedles induces hair regrowth, *Biomaterials* 167 (2018) 69–79, <https://doi.org/10.1016/j.biomaterials.2018.03.019>.
- [63] C.Y. Janda, L.T. Dang, C. You, J. Chang, W. de Lau, Z.A. Zhong, K.S. Yan, O. Marecic, D. Siepe, X. Li, et al., Surrogate Wnt agonists that phenocopy canonical Wnt and β -catenin signalling, *Nature* 545 (7653) (2017) 234–237, <https://doi.org/10.1038/nature22306>.
- [64] S. Bonnet, R. Paulin, G. Sutendra, P. Dromparis, M. Roy, K.O. Watson, J. Nagendran, A. Haromy, J.R.B. Dyck, E.D. Michelakis, Dehydroepiandrosterone reverses systemic vascular remodeling through the inhibition of the akt/GSK3- β /NFAT Axis, *Circulation* 120 (13) (2009) 1231–1240, <https://doi.org/10.1161/CIRCULATIONAHA.109.848911>.
- [65] C.E. Meacham, A.W. DeVilbiss, S.J. Morrison, Metabolic regulation of somatic stem cells in vivo, *Nat. Rev. Mol. Cell Biol.* 23 (6) (2022) 428–443, <https://doi.org/10.1038/s41580-022-00462-1>.
- [66] A. Flores, J. Schell, A.S. Krall, D. Jelinek, M. Miranda, M. Grigorian, D. Braas, A. C. White, J.L. Zhou, N.A. Graham, et al., Lactate dehydrogenase activity drives hair follicle stem cell activation, *Nat. Cell Biol.* 19 (9) (2017) 1017–1026, <https://doi.org/10.1038/ncb3575>.
- [67] S.N. Shapira, H.R. Christofk, Metabolic regulation of tissue stem cells, *Trends Cell Biol.* 30 (7) (2020) 566–576, <https://doi.org/10.1016/j.tcb.2020.04.004>.